Received: 9 December 2024 | Revised: 7 March 2025 | Accepted: 10 September 2025 | Published online: 22 September 2025

RESEARCH ARTICLE

Journal of Data Science and Intelligent Systems
2025, Vol. 00(00) 1–9
DOI: 10.47852/bonviewJDSIS52024990

BON VIEW PUBLISHING

Using Test Trials of Processing Systems for Non-Blind Recovery of Signals and Images

Andrey V. Novikov-Borodin[1,*]

[1]*Institute for Nuclear Research, Russian Academy of Sciences, Russia*

Abstract: The mathematical method for non-blind recovery of one-dimensional and multidimensional signals, including images, distorted during processing by linear stationary (or time-invariant) systems is considered. Instead of transfer functions, which are often difficult to determine because they belong to the class of generalized functions, the proposed method uses test trial signals of processing systems for signal recovery. Unlike the transfer functions, the test signals belong to the class of ordinary functions, which simplifies the signal reconstruction procedure considerably and makes it more accurate and stable. It also allows existing methods, such as regularization technique, to be effectively used to solve ill-posed and ill-conditioned problems for recovering nondeterministic signals with high levels of noise and uncertainty. The proposed operator approach based on the multidimensional convolution equation significantly reduces the number of operations and increases the speed of numerical computations. The considered method allows improving the quality of signal and image processing without complex and expensive modernization of the equipment.

Keywords: mathematical recovery, non-blind methods, test trials of processing systems, multidimensional convolution equation, ill-posed and ill-conditioned problems

1. Introduction

Real processing systems are imperfect, resulting in distortion and noise in the processed signals. Hardware methods of distortion suppression require solving complex scientific and technical problems and creating expensive equipment. Alternative mathematical methods use special transformations to recover undistorted data from distorted and noisy ones. Recovery problems are usually ill-posed and often ill-conditioned [1–4], so there are no universal methods for their solution, and developing methods that are effective in specific cases is an urgent challenge.

In this paper, we consider the recovery of data distorted during processing by linear stationary (LS) (or linear time-invariant) systems. Data transformations by these systems satisfy the convolution-type equations, so data distortions are determined by their transfer functions ([5] and Section 2). In various fields of science, transfer functions are also called as hardware or system functions, system distortions, distortion kernels, superposition functions, point spread functions, etc. Noise and uncertainties in real nondeterministic signals can be considered as a random part of signal distortions (for details, see the model of signal processing in Section 2).

When the distortion kernels and/or noise distributions are known, non-blind deconvolution methods can be used to recover undistorted data from distorted ones [6–14]. However, processing systems are quite different, and their transfer functions and noise distributions in signals are very diverse and usually unknown. Transfer functions often belong to the class of generalized functions [5] and Section 2 for details), so they are quite difficult not only to identify but also to represent. It follows that non-blind methods are typically used on a small set of blur kernels and noise distributions.

Blind methods do not require direct identification of distortion functions, but they use a priori knowledge or assumptions about the original or desired appearance of the recovered data, their parts, and/or structure [15–17]. However, also as in the previous case, it is quite difficult to get this information for very diverse processing systems, signals, and noise distributions. It severely limits the scope of blind methods, which are mainly used to reconstruct images in which object representations can be systematized.

The use of neural networks also avoids direct determination of transfer functions, but neural networks are trained on a large number of samples, and in many cases, such averaging does not provide high accuracy of data reconstruction [18–21].

The reconstruction method proposed in this paper can be used in areas where the considered existing methods are ineffective or fail. This method can be categorized as non-blind because it relies on the exact correspondence of input and output data within certain physical constraints. However, it does not require transfer or distortion functions, but instead uses the test trial signals of the processing systems. Unlike transfer functions, test signals (TS) belong to ordinary functions, so defining and representing them is not difficult. Furthermore, in the absence of generalized functions, various methods can be effectively used to solve ill-posed and ill-conditioned problems of recovering real nondeterministic signals with high levels of noise and uncertainties. In this paper, we use the regularization technique [22, 23], but many other methods (e.g., iterative or wavelet) can also be used.

Unlike previous works [24, 25], which introduced the idea of using test trial signals in the reconstruction process, this paper

*Corresponding author: Andrey V. Novikov-Borodin, Institute for Nuclear Research, Russian Academy of Sciences, Russia. Email: novikov@inr.ru

proposes a model of processing by LS systems of nondeterministic signals with noise and uncertainties. This model allows us to analyze in detail the basic equation for signal recovery, called the test trial equation. The analysis proved that the test trial equation has a low level of uncertainty, which predetermines the stability of the algorithm and the recovery efficiency of the highly noisy data. Also in contrast to previous works [24, 25], an operator approach based on the multidimensional convolution equation is used instead of the matrix approach to recover the signals in the spatial domain. This significantly speeds up numerical computations, reducing the number of required operations from $\sim 5n^3$ to $\sim 5n^2$ when recovering big data sets of n elements. These program codes and related datasets are openly placed on GitHub.

The numerical experiments presented in this paper demonstrate the capabilities of the proposed method for the reconstruction of one-dimensional signals in the spatial domain and two-dimensional images in the spectral domain. In the first example, the effective bandwidth of the processing system, which is a capacitive voltage divider, was increased by three orders of magnitude, from 1 MHz to about 1 GHz. This example also demonstrates the stability of the algorithm at high levels of noise and uncertainties in signals. To illustrate the algorithm of recovery of multidimensional signals in the spectral domain, an example of recovery of a fractal image distorted by a random two-dimensional kernel with discontinuities is given.

2. Test Trial Equation

A processing system is LS, if in a region $x \in D$ its response $w(x)$ (output signal) to an external action $v(x)$ (input signal) corresponds to a convolution-type equation [5], which we will call the LS system equation, or, for short, the LS equation:

$$w(x) - \{\eta(x)\} = (u * v)(x) = \int_D u(x-\xi)v(\xi)\mathrm{d}\xi. \qquad (1)$$

Here $u(x)$ is an LS system transfer function characterizing its operation and $\eta(x) = (\Delta w - u * \Delta v - \Delta u * v + \Delta u * \Delta v)(x)$ is the LS equation uncertainty. The LS equation follows from the convolution equation:

$$w_0(x) = (u_0 * v_0)(x)$$

for the corresponding deterministic functions without uncertainties $w_0(x) = (w - \Delta w)(x)$, $u_0(x) = (u - \Delta u)(x)$, and $v_0(x) = (v - \Delta v)(x)$ shown in Figure 1.

By introducing the convolution operator $\mathcal{F}$ generated by a function $f(x)$: $\mathcal{F}g(x) \equiv (f * g)(x)$, we can represent the LS equation in the operator form:

$$\mathcal{U}v(x) = w(x) - \eta(x)$$

or, by using the Borel's convolution theorem, in its spectral domain:

Figure 1
Signal processing by the LS system

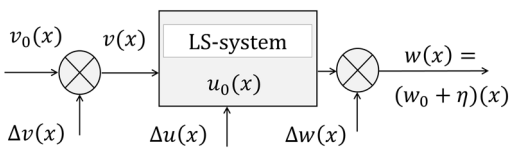

$$U(\omega)V(\omega) = W(\omega) - \{\mathcal{N}(\omega)\}.$$

Here $F(\omega) = FT[f(x)]$ is the spectrum (Fourier transform) of the function $f(x)$ and $\mathcal{N}(\omega) = \Delta W(\omega) - U(\omega)\Delta V(\omega) - \Delta U(\omega)V(\omega) + \Delta U(\omega)\Delta V(\omega)$. Note that the spectrum of introduced convolution operator coincides by definition with the spectrum of its generating function ($F(\omega) = FT[f(x)] = FT[\mathcal{F}]$).

It is possible to reconstruct the spectrum of the input signal by dividing both parts of the LS equation spectral form by the spectrum of the transfer function, but only if: $|U(\omega)| \neq 0$. When the uncertainties in the transfer function are random with zero mean deviation: $\langle \Delta U \rangle = 0$, then: $\langle U \rangle = \langle U_0 \rangle$, and it can be expected that the spectrum $V(\omega)$ can be recovered only inside the frequency region, which we will call the expected frequency reconstruction range (FR range) of the LS equation:

$$\Omega_{LS}^V = \Omega_U^V = \{\omega : \ |U_0(\omega)| \neq 0\}.$$

This region corresponds to the LS system bandwidth. It is also possible to use the confidence range, within which the spectrum amplitude of the LS equation uncertainty is smaller than the spectrum amplitude of the transfer function: $\Omega_U^V = \{\omega : |U_0(\omega)| > \gamma|\mathcal{N}(\omega)|\}$, where $\gamma \geq 0$ is a confidence coefficient, but further for simplicity of estimations we will use the FR range.

LS systems can also be described by an ordinary differential equation with constant coefficients a_k: $w(x) = \sum_{k=0}^n a_k v^{(k)}(x)$. Indeed, for locally integrable functions: $v^{(k)}(x) = \left(\delta^{(k)} * v\right)(x)$, where $\delta^{(k)}$ is the k-th derivative of the delta function, so using linearity and associativity of convolution, we obtain:

$$w(x) = \sum_{k=0}^n a_k v^{(k)}(x) = \sum_{k=0}^n a_k \left(\delta^{(k)} * v\right)(x) =$$

$$= \left(\left(\sum_{k=0}^n a_k \delta^{(k)}\right) * v\right)(x) = (u * v)(x).$$

Thus, the transfer functions of such LS systems are equal to the sum of derivatives of the δ-function: $u(x) = \sum_{k=0}^n a_k \, \delta^{(k)}(x)$, so, in general, they belong to the class of generalized functions. In this case, for real nondeterministic signals, the determination of the transfer function $u_0(x)$ from the TS equation:

$$(u_c * v_c)(x) = w_c(x) - \{\eta_c(x)\}, \qquad (2)$$

where $w_c(x)$ is the response of the LS system to some test action $v_c(x)$, and $\eta_c(x) = (\Delta w_c - u_c * \Delta v_c - \Delta u_c * v_c - \Delta u_c * \Delta v_c)(x)$ and $u_c(x) = (u_0 + \Delta u_c)(x)$ (see Figure 1), can be a much more difficult task than recovering signals belonging to the class of main functions.

It is possible to avoid many problems associated with the use of transfer functions by eliminating them from consideration. Let's convolve both parts of TS equation (2) with action $v(x)$, and LS equation (1) with test action $v_c(x)$:

$$\begin{cases} (v * w_c)(x) = (v * (u_c * v_c))(x) + \{(v * \eta_c)(x)\}, \\ (v_c * w)(x) = (v_c * (u * v))(x) + \{(v_c * \eta)(x)\}. \end{cases}$$

Subtracting the second equation from the first one and given that: $(u_c - u)(x) = (u_0 + \Delta u_c - u_0 - \Delta u)(x) = (\Delta u_c - \Delta u)(x)$, we obtain the test trial (TT) equation:

$$(w_c * v)(x) = (v_c * w)(x) - \{\eta_T(x)\}, \qquad (3)$$

where $\eta_T(x) = (v_c * (\Delta w + v * \Delta u) - v * (\Delta w_c + v_c * \Delta u_c))(x)$. In the spectrum domain the TT equation is:

$$W_c(\omega)V(\omega) = V_c(\omega)W(\omega) - \{\mathcal{N}_T(\omega)\}.$$

Formally, the expected FR range of reconstructing the input signal $v(x)$ from the TT equation $\Omega_{TT}^V = \{\omega : |W_0^c(\omega)| \neq 0\}$ is the same as the expected FR range Ω_{LTS}^V of reconstructing this signal from the LS equation and determining the transfer function $u(x)$ from the TS equation. Indeed, $\Omega_{TT}^V = \{\omega : |U_0(\omega)V_0^c(\omega)| \neq 0\} = \Omega_{LS}^V \setminus \Omega_{TS}^U = \Omega_{LTS}^V$. However, the error of reconstruction of the action $v(x)$ from LS and TS equations also includes the error of representing the transfer function, which can be very large if the transfer function is a generalized one.

Substituting the expressions for $\eta(x)$ and $\eta_c(x)$ from Equations (1) and (2) into $\eta_T(x)$, we see that the terms $v * \Delta u$ and $v_c * \Delta u_c$ are reduced:

$$\eta_T(x) = (v_c * (\Delta w - u * \Delta v + \Delta u * \Delta v) -$$

$$- v * (\Delta w_c - u_c * \Delta v_c + \Delta u_c * \Delta v_c))(x),$$

which follows the reducing the expected error of signal reconstruction from the TT equation.

Considering further that $u(x) = (u_0 + \Delta u)(x)$ and $u_c(x) = (u_0 + \Delta u_c)(x)$, one can see that the uncertainty

$$\eta_T(x) = (v_c * (\Delta w - u_0 * \Delta v) -$$

$$- v * (\Delta w_c - u_0 * \Delta v_c))(x)$$

does not depend explicitly on the uncertainties $\Delta u(x)$ and $\Delta u_c(x)$ in the transfer function, which follows the stability of the recovery algorithm from the TT equation.

Thus, the TT equation does not contain transfer functions, so there are no problems with the determination and representation of generalized functions. The determination and representation of LS system signals belonging to ordinary functions is not difficult since both numerical and experimental methods can be used. This ensures the versatility of the proposed approach, the stability of its algorithm, and accuracy when recovering highly noisy data.

Note that when TSs are determined experimentally, there is no need to analyze the LS system and also the parasitic parameters of its elements, since this information is provided in the TSs. This allows recovering signals of high-speed and precise processing systems of almost any complexity and structure. Note also that signals of LS systems can be of any type. For example, they can be electrical signals or physical fields acting on, measured, or generated by the processing system.

3. Solutions to TT equation

The TT equation is a convolution-type equation and, according to regularization theory [22, 23], its solution $v_r(x)$ is the function minimizing the functional $\Phi[v] = ||\mathcal{V}_c w - \mathcal{W}_c v||^2 + \lambda||\mathcal{P}v||^2$ with stabilizer $\lambda||\mathcal{P}v||^2$, where $\mathcal{P}$ is the operator corresponding to the constraints imposed on the reconstructed function $v(x)$, and λ is the regularization parameter. Equating to zero the variation of this functional on v, we obtain:

$$v_r(x) = (\mathcal{W}_c^+\mathcal{W}_c + \lambda\mathcal{P}^+\mathcal{P})^{-1}\mathcal{W}_c^+\mathcal{V}_c w(x), \tag{4}$$

where $\mathcal{F}^+$ is a conjugate-transpose operator to the operator $\mathcal{F}$. The spectral form of this solution is:

$$V_r(\omega) = \frac{W_c^+(\omega)V_c(\omega)W(\omega)}{W_c^+(\omega)W_c(\omega) + \lambda P^+(\omega)P(\omega)}.$$

In the multidimensional case, it is possible to consider the equality $FT(\mathcal{F}^+\mathcal{F}) = F^+(\omega)F(\omega)$ as a definition of the conjugate-transpose operator.

The optimal stabilizer for real-valued functions with random uncorrelated uncertainties commonly encountered in practice corresponds to the Wiener filter: $\lambda P^+(\omega)P(\omega) = |\mathcal{N}_T(\omega)|^2/|V(\omega)|^2$, where the power spectra $|\mathcal{N}_T(\omega)|^2$ and $|V(\omega)|^2$ of random stationary processes are understood as expected values.

The Wiener stabilizer is usually unknown, but since it is non-negative and symmetric for real-valued functions, one can search it in the form of a non-negative symmetric function, e.g., as a polynomial: $\lambda P^+(\omega)P(\omega) = \sum_{k=0}^n \lambda_k \omega^{2k}$ considering the non-negative coefficients $\lambda_k \geq 0$ as regularization parameters. According to the Fourier transform for derivatives, this representation corresponds to solutions having $2k$ order derivatives with a "degree of continuity" determined by the values of λ_k. Consequently, the widest class of solutions with "degree of continuity" determined by the value of λ_0 gives a zero-order stabilizer ($n = 0$): $P^+(\omega)P(\omega) = \lambda_0$ or $\mathcal{P}^+\mathcal{P} = \lambda_0\mathcal{J}$, where $\mathcal{J}$ is an identity operator.

According to regularization theory, the residual $||(v_c * w - w_c * v_r(\lambda))(x)||$ increases monotonically with increasing of λ, so the optimal values of λ can be found from the equation: $||(v_c * w - w_c * v_r(\lambda))(x)|| = ||\eta_T(x)||$. Therefore, the necessary condition for recovering signals from the TT equation is: $||\eta_T(x)|| \leq ||(v_c * w - w_c * v)(x)||$.

Let the functions $g(x)$, $f(x)$ and $h(x)$: $g(x) = (f * h)(x)$ be represented as M-dimensional arrays $\boldsymbol{g} = \{g_{i_1..i_M}\}$, $\boldsymbol{f} = \{f_{i_1..i_M}\}$ and $\boldsymbol{h} = \{h_{i_1..i_M}\}$ on the grid $\{d_{i_1....i_M}\}$, $i_k = 0..m_k - 1$, $k = 1..M$, partitioning the rectangular region $D_0 \supseteq D$. From Equation (1) for the element $g_{i_1..i_M} = g(d_{i_1..i_M})$ we have: $g_{i_1..i_M} = \int_{D_0} f(\xi)h(d_{i_1..i_M} - \xi)\mathrm{d}\xi$. The partial sum of this integral on the grid $\{d_{i_1..i_M}\}$:

$$g_{i_1..i_M} \approx \sum_{j_1=0}^{m_1-1} \cdots \sum_{j_M=0}^{m_M-1} f_{j_1..j_M} h_{i_1-j_1,..,i_M-j_M} \Delta_{j_1..j_M} \tag{5}$$

is exactly the discrete convolution equation if the array f is redefined as $f_{j_1..j_M} = f_{j_1..j_M}\Delta_{j_1..j_M}$, where $\Delta_{j_1..j_M}$ is the volume element. Being the partial sum of the integral, Equation (5) contains the errors associated with data discretization.

Considering Equation (5) as a convolution operator of multidimensional discrete data: $\boldsymbol{g} = \mathcal{F}\boldsymbol{h} = \boldsymbol{f} * \boldsymbol{h}$, we obtain from Equation (2) the TT equation in the discrete form:

$$\mathcal{V}_c\boldsymbol{w} = \mathcal{W}_c\boldsymbol{v} - \{\boldsymbol{\eta}_T\}. \tag{6}$$

On a uniform partitioning grid, one can reduce the volume elements in both parts of this equation, so, unlike Equation (5), no function redefinition is required here. From Equation (4), we obtain the discrete regularized solution of the TT equation in the operator form:

$$\boldsymbol{v}_r = (\mathcal{W}_c^+\mathcal{W}_c + \lambda\mathcal{P}^+\mathcal{P})^{-1}\mathcal{W}_c^+\mathcal{V}_c\boldsymbol{w} \tag{7}$$

and in the spectral form:

$$V^r_{j_1..j_M} = \frac{W^{c+}_{j_1..j_M} V^c_{j_1..j_M} W_{j_1..j_M}}{W^{c+}_{j_1..j_M} W^c_{j_1..j_M} + \lambda P^+_{j_1..j_M} P_{j_1..j_M}}.$$

The number of operations required to recover arrays with n elements using the operator Equation (7) based on the discrete convolution Equation (5) can be estimated as: $N(n) \sim \mathrm{O}(5n^2 + n + N(\lambda\mathcal{P}))$, which is much faster for large n than the matrix approach used earlier in Novikov-Borodin [24, 25], which required $\sim 5n^3$ operations. When using the spectral form of Equation (7) (with direct and inverse DFT), the required number of operations is: $N(n) \sim \mathrm{O}(4n\log(n) + n + N(\lambda P))$. Here, $N(\lambda\mathcal{P})$ and $N(\lambda P)$ are the number of operations with stabilizers.

Numerical calculations in the spectral domain are much faster than in the spatial domain. However, signals are usually considered in limited spatial or time regions, outside of which they are unknown. In this case, if the signals in the outer regions are non-zero and non-periodic, their spectra depending on Fourier transform over a hole space cannot be determined. This circumstance significantly limits the scope of the application of spectral methods and makes calculations in the spatial domain relevant and in demand.

4. Test Signals

As mentioned in Section 2, the expected frequency range of the TT equation $\Omega^V_{TT} = \{\omega : |U_0(\omega)V^c_0(\omega)| \neq 0\}$ directly affects the reconstruction error, so to decrease this error, the expected frequency range of the test action $\Omega^c_V = \{\omega : |V^c_0(\omega)| \neq 0\}$ should exceed the expected frequency range of the reconstructed signal $\Omega_V = \{\omega : |V_0(\omega)| \neq 0\}$ and/or the bandwidth of the processing system $\Omega_U = \{\omega : |U_0(\omega)| \neq 0\}$. To decrease the term $\{\mathcal{N}_T(\omega)/W^c_0(\omega)\}$ (see Equation (3)) one also needs to increase the amplitude of the test action spectrum. Since the term $\mathcal{N}_T(\omega)$ is random and can have a very wide frequency range, the amplitude of the spectrum of an ideal test action should be large and uniform over the widest possible frequency space. However, this is the spectrum of a delta function, which has zero width and infinite amplitude, so it cannot be realized in practice.

Consider some approximation to the one-dimensional delta function in the form of a trapezoidal pulse with the amplitude A, duration T, leading b, and trailing B edges: $r(t) = A\,t/b$ at $t \in [0, b]$, A at $t \in [b, T+b]$, $A(T+b+B-t)/B$ at $t \in [T+b, T+b+B]$. The amplitude of the spectrum $R(\omega) = |FT(r(t))|$ of this pulse is equal to:

$$R(\omega) = \frac{A}{|\omega|}\left|\frac{\sin\left(\frac{\omega b}{2}\right)}{\frac{\omega b}{2}} - \frac{\sin\left(\frac{\omega B}{2}\right)}{\frac{\omega B}{2}}e^{-I\phi}\right|, \tag{8}$$

where $\phi = \omega(T + (B+b)/2)$ and I is an imaginary unit.

When $B = b$, $R(\omega)$ has a lot of zeros on the frequency axis, which reduces the frequency range of the signal. One can extend this range by decreasing the duration T, but this results in a proportional decrease in the amplitude of the spectrum. It is possible to achieve best results by adjusting the duration of the pulse edges.

Figure 2a shows trapezoidal pulses $r(t)$ with peak duration $T = 10$ ns, leading edge $b = 1$ ns, various trailing edges $B = b$ [1] (red lines), $B = \pi b$ [2] (blue lines), $B = 4\pi b$ [3] (green lines), and spectrum amplitudes $R(\nu)$, $\nu = \omega/2\pi$ GHz, of these pulses. When the edges are equal $B = b = 1$ ns [1], the amplitude of the pulse spectrum has many zeros on the frequency axis. As the trailing edge B increases, the summands in Equation (8) are zero at different frequencies $\omega_k = 2\pi k/b$ and $\omega_m = 2\pi\, m/B$, where k, m are non-zero integers, and when B/b is an irrational number, these summands do not simultaneously go to zero on the entire frequency axis. As the trailing edge increases to $B = \pi b$ [2], the dips in the spectrum amplitude are decreasing and at $B = 4\pi b$ ($B \gg b$) [3] smooth out to small oscillations around the main trend defined by the first term in the Equation (8).

With further increasing B, the zeros of the first term in Equation (8) are less compensated by the second term. In the limit, when $B \to \infty$, we obtain the TS as a step function with leading edge b, whose spectrum amplitude determined by the first term in Equation (8) has a maximum value in the low-frequency region, but the zeros of the first term are not compensated by the second term. In addition, the step function is unbounded on the right-hand side, which leads to problems when considering signals at finite intervals, for example, in numerical calculations. Thus, the relations $B \approx T \gg b$ can be considered optimal for trapezoidal test pulses.

One can come to similar conclusions in the case of trapezoidal-like pulses with nonlinear edges, for example, with Gaussian edges: $g(t) = A\exp(-(t-b)^2/2b^2)$ at $t \le b$, A at $b < t \le T$, $A\exp(-(t-T)^2/2B^2)$ at $t > T$, or with exponential ones: $e(t) = A\,(1-\exp(-t/b))/(1-\exp(-T/b))$ at $0 < t \le T$, $A\exp(-(t-T)/B)$ at $t > T$. Figure 2b and c show the pulses $g(t)$ and $e(t)$ and their spectrum amplitudes $G(\nu)$ and $E(\nu)$ at $B = b$ [1], $B = \pi b$ [2], and $B = 4\pi b$ [3]. As before, the ratios $B \approx T \gg b$ are optimal for reducing the dips in the spectrum amplitude and extending the frequency range of the TSs.

The amplitude distribution of the spectrum of pulses with exponential edges is more uniform than with linear ones and decreases with increasing frequency not as fast as for pulses with Gaussian edges. Pulses with exponential and Gaussian edges are not limited on the right-hand side, which can cause problems when recovering signals at finite intervals. For nondeterministic signals, one can consider finite intervals beyond which the level of signals is less than the level of uncertainties in them. The frequency range of nondeterministic signals is determined up to dips of amplitudes of their spectra to amplitudes of uncertainty spectra.

In the multidimensional case, it is possible to use TSs in the form of a direct product of the considered one-dimensional TSs, e.g., $v_c(x) = e(x_1) \times r(x_2) \times \cdots \times e(x_n)$.

5. Examples of Reconstruction

The results of the numerical experiment on recovery of one-dimensional signals $v_0(t) = (\nu - \Delta\nu)(t)$ of complex shape (superposition of trapezoidal and Gaussian pulses) at the input of the capacitive voltage divider from the distorted output signal $w(t)$ using the TSs $w_c(t)$ and $v_c(t)$ are presented in Figure 3. A trapezoidal-like pulse with different exponential edges was used as the test action $v_c(t)$, providing a wide signal spectrum (see Section 4 for details). The circuit diagram of the divider was taken from the standard library of Micro-CAP 12.2.0.4 analog/digital circuit simulator of Spectrum Software. The signals were also calculated using this program. For visibility, the output signals are shown with a scaling factor compensating the voltage drop across the divider.

All signals on the interval from 0 to 250 ns were transformed into vectors $\boldsymbol{w}$, $\boldsymbol{v}$, $\boldsymbol{v}_0$, $\boldsymbol{w}_c$, $\boldsymbol{v}_c$ of size $n = 500$ with sampling step $\Delta = 0.5$ ns. The operator Equation (7) with a zero-order stabilizer $\lambda_0\mathcal{J}$ was used for the searching the widest class of solutions with the "degree of continuity" determined by the parameter λ_0. Without additional noise in the signals, the relative error of the $\boldsymbol{v}_r$ reconstruction of the $\boldsymbol{v}_0$ signal at the sample points was $\delta\boldsymbol{v}_r = ||\boldsymbol{v}_r - \boldsymbol{v}_0||/||\boldsymbol{v}_0|| = 0.23$ %. The results $\boldsymbol{v}_r$ of reconstruction of signal $\boldsymbol{v}_0$ in the presence of additional Gaussian noise with dispersion 5 and 10 % of the maximum values of signals $\boldsymbol{v}$, $\boldsymbol{v}_c$ and $\boldsymbol{w}$, $\boldsymbol{w}_c$ are shown in Figure 3b and c. The relative reconstruction errors $\delta\boldsymbol{v}_r$ in these cases were 1.73 and 2.93 %.

Figure 2
Test signals and their spectrum amplitudes

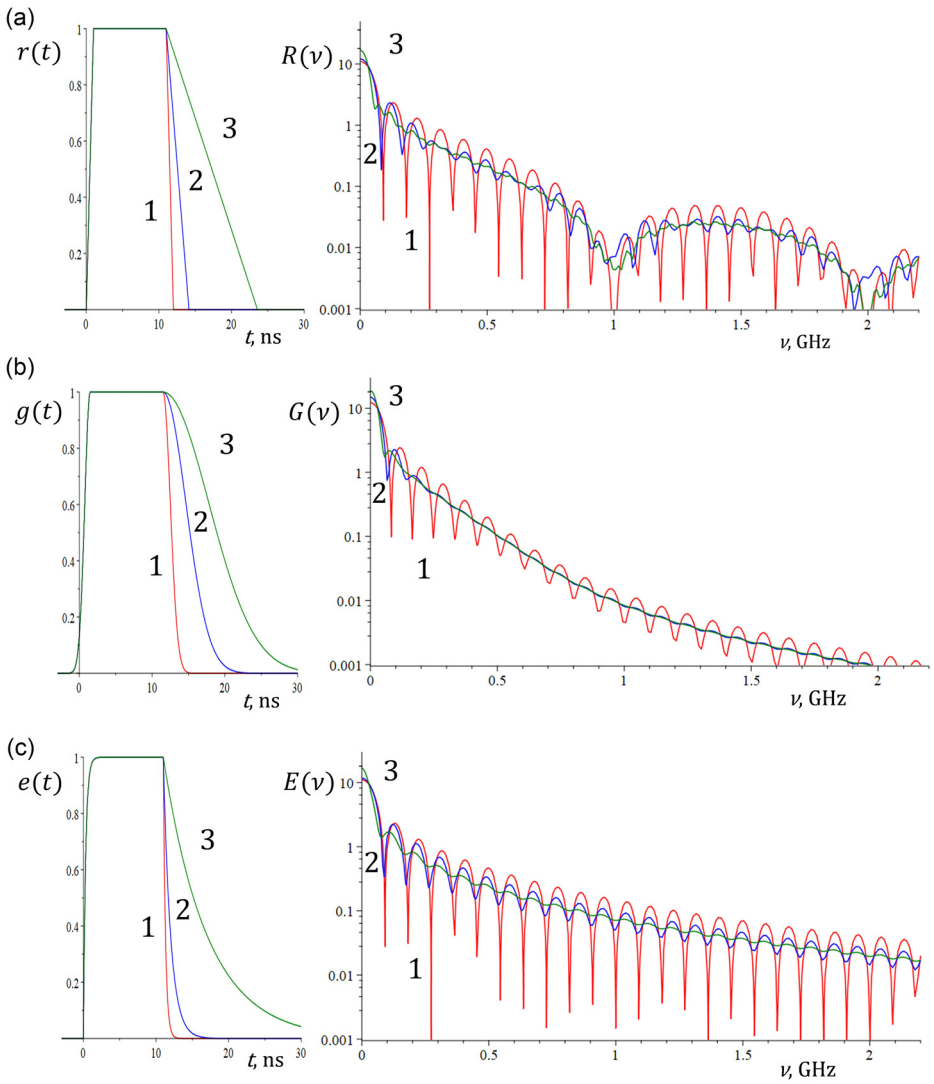

In the considered example, the divider cutoff frequency was 1 MHz, but using the proposed mathematical method we were able to register the signals with nanosecond edges. In fact, the proposed method allows us to increase the effective bandwidth of the processing system by three orders of magnitude from 1 MHz to ∼ 1 GHz.

Numerical calculations were performed in the Maple 2017.3 Waterloo Maple Inc. environment on an HP 255 G7 laptop with an AMD Ryzen 3, 2.5 GHz processor. Program codes and data sets are available in GitHub at https://github.com/novikov-borodin/data-rec/signal-rec. The recovery time for discrete signals of size $n = 501$ corresponding to a sampling step $\Delta = 0.5$ ns was 1.6..2.0 s. For data of size $n = 251$ ($\Delta = 1.0$ ns), the computation time was 0.4 . . . 0.5 s, which is in a good agreement with the earlier estimates of the quadratic dependence of the number of operations in Section 3 (see comments to Equation (7)).

The nonlinear slowing down of the reconstruction error growth with increasing noise level in the data can be explained by efficient smoothing of the growing high-frequency noise spectrum during regularization of the solution. In general, the reconstruction error is random, since it depends not only on the noise level but also on the random noise distributions in the data. Figure 4 illustrates the dependence of the relative reconstruction error $\delta \boldsymbol{v}_r$ % on the relative noise level $\delta \boldsymbol{w}$ % in the output signal. The dots show the reconstruction errors obtained in numerical experiments. The curve $\langle \delta \boldsymbol{v}_r \rangle$ is the expected value of reconstruction errors, the curves $\delta \boldsymbol{v}_{min}$ and $\delta \boldsymbol{v}_{max}$ show the expected range of these errors. The noise levels in the TSs in Figure 4 were $\delta \boldsymbol{w}_c = 2.2$ % and $\delta \boldsymbol{v}_c = 1.4$ %.

Figure 5 illustrates the reconstruction of multidimensional signals in the spectral domain. Note that images are only a special case of multidimensional signals because images are usually composed of objects, so they have some predefined properties and structure. Multidimensional signals in general do not have such properties. Thus, a fractal image $\boldsymbol{v}$ with different scales of objects is chosen for reconstruction only for clarity. Figure 5 shows the result of recovering $\boldsymbol{v}_r$ of the color image $\boldsymbol{v}$ of size 500 × 700 pixels in *jpeg* format from the image $\boldsymbol{w}$ of size 549 × 769 blurred with a kernel $\boldsymbol{u}$ of size 50 × 70 using the spectral representation of Equation (7). The distortion kernel $\boldsymbol{u}$ is not required for reconstruction, and it is presented in Figure 5 for clarity to show that it is a random two-dimensional kernel with discontinuities.

For simplicity, the distortions were the same for all three-color layers, so it was sufficient to use grayscale test images $\boldsymbol{w}_c$ and $\boldsymbol{v}_c$ in

Figure 3
Reconstruction of 1D signals

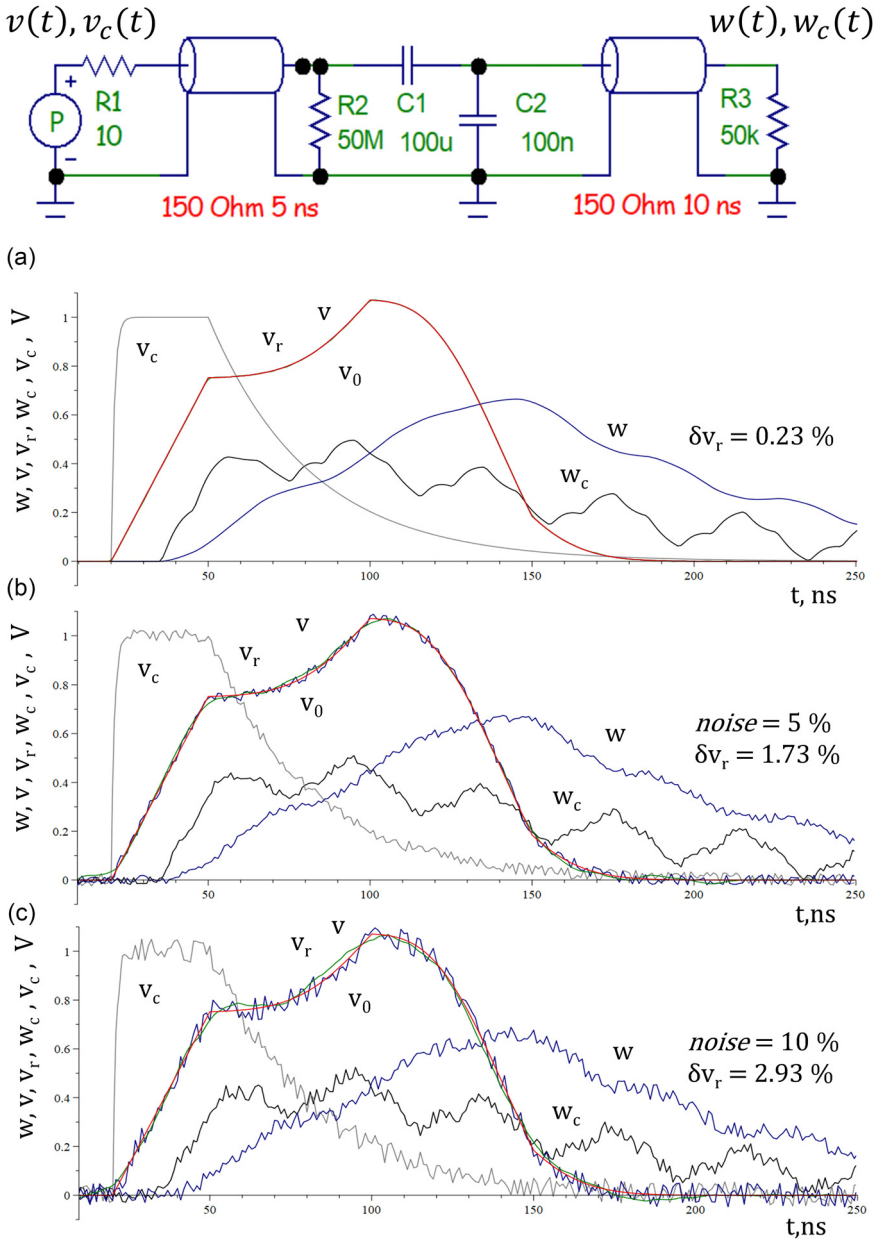

for reconstruction. Otherwise, color test images and a color distortion kernel would have been required. The test image $\boldsymbol{v}_c$ is a direct product of trapezoidal signals with exponential edges (see Section 4 for details). The relative error of image reconstruction without additional noise in the data is $\delta\boldsymbol{v}_r = |\boldsymbol{v}_r - \boldsymbol{v}_0|/|\boldsymbol{v}_0| = 4.23 \cdot 10^{-10}$ %. When random noise with normal distribution with variance 0.1 and 0.05 is added to the output signals w and w_c, the reconstruction error increases to $\delta\boldsymbol{v}_r = 2.30$ %.

In general, different image reconstruction quality estimates cannot be used for multidimensional signals, so the statistical distribution of error bars $|\boldsymbol{v}_r - \boldsymbol{v}_0|$ is presented in Figure 5. The errors are maximal (white areas) at sharp edges of the image objects.

Calculations were made in the Maple 2017.3 environment of Waterloo Maple Inc. Program codes and data sets are available in GitHub at https://github.com/novikov-borodin/data-rec/image-rec.

The recovery time of the color *jpeg* image (with three layers) of 500×700 pixels size shown in Figure 5 was 127.2 s, which corresponds to the computation time of each layer $t = 127.2/3 = 42.4$ s. The recovery time of the grayscale *jpeg* image (with one layer) of size 201×201 pixels was $t_2 = 4.453$ s. Recalculating the recovery time $t = t_2 N(n)/N(n_2) = 42.55$ s (≈ 42.4 s) shows a good agreement with the estimates of the required number of operations given above in Section 3.

6. Discussions

The test trial method proposed in this paper has been classified as non-blind, because within some physical constraints, it uses an exact correspondence between the input and output signals. However, the TT method does not utilize transfer or distortion

Figure 4
Reconstruction errors versus noise level in the signals

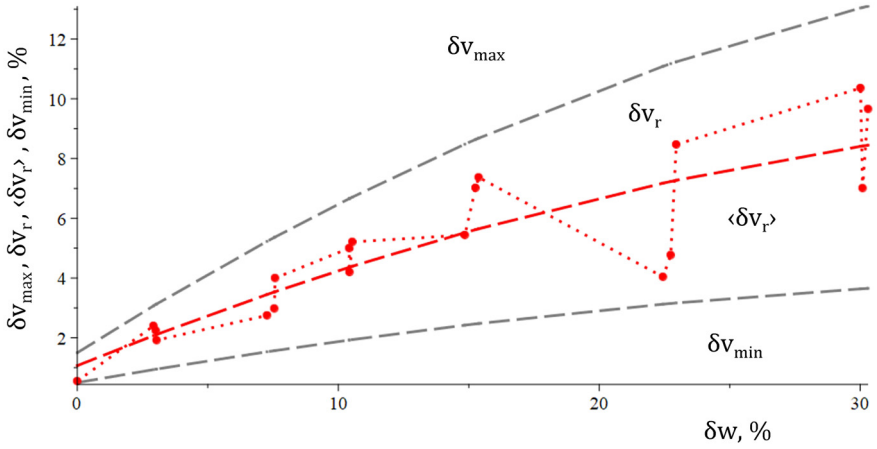

Figure 5
Image recovery

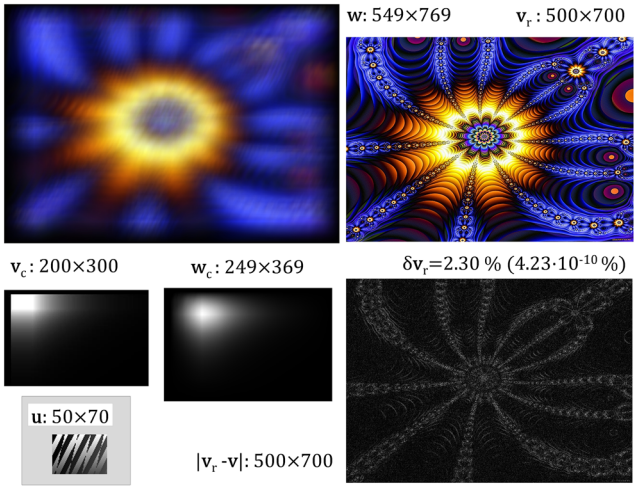

functions, so formally it can also be categorized as blind. Moreover, one can consider the described test trial of processing system as a single but effective training of a neural network for signal recovery. It seems that exactly these mixed features predetermine the advantages of the TT method and its effective use in areas where other methods are ineffective or do not work. For example, when the transfer or distortion functions are unknown and belong to the class of generalized functions.

Thus, the main achievement of TT methods is the expansion of the field of application of mathematical reconstruction methods. However, exactly this advantage leads to difficulties in comparing TT methods with others. Indeed, how to compare methods with different fields of application? And, how do you quantitatively compare TT methods with others if they don't use TSs and they are not presented in papers? We found only one reference with estimates suitable for comparison. A plenary report [26] reviewing the general capabilities of signal recovery in measurement systems concluded that existing mathematical methods they used, including neural networks, can improve the quality of processing systems (e.g., effective bandwidth) by a factor of 1.5–2. Nevertheless, in a numerical experiment (Figure 3 in Section 5), we increased the effective bandwidth of the processing system by three orders of magnitude from 1 MHz to ~1 GHz using TT methods. In this example, we also demonstrated the robustness of the proposed reconstruction algorithm under high levels of noise and uncertainty in the signals (Figures 3 and 4).

In fact, the test trials of the processing systems are their extended calibration or their dynamic calibration in the one-dimensional case. Exactly this extended calibration provides an opportunity to improve the effective parameters of the processing systems. From this point of view, the proposed TT method is a technique for using the TSs of the processing systems to restore the signals distorted by them.

The basic equation for signal reconstruction – the TT equation (3) – is a standard convolution-type equation, but it does not contain the generalized functions, which allows the efficient use of many existing methods. We used the regularization technique to illustrate the capabilities of the TT method while preserving its versatility using a zero-order stabilizer (see Section 3 for details). However, various methods can also be used to solve the TT equation. That is why we do not consider the regularization technique to be an integral part of the TT method. In some specific cases, other methods may be more efficient. This is another reason why it is difficult to compare the TT approach with other methods. Although we do not consider methods for solving TT equations to be an integral part of the TT approach, from the resulting point of view, solving ill-posed and ill-conditioned reconstruction problems remains one of its main problems.

Signal reconstruction is possible in both spatial and spectral domains. Numerical calculations in the spectral domain are much faster than in the spatial domain, even taking into account the direct and inverse Fourier transforms. However, in practice, signals are usually considered in limited spatial or time regions, outside of which they are unknown. In this case, if the signals in the outer regions are non-zero and non-periodic, their spectra depending on Fourier transform over a hole space cannot be determined. This circumstance significantly limits the scope of application of spectral methods and makes calculations in the spatial domain relevant and in demand.

The TT method operates under the assumption that the processing system is linear and stationary, so in general, small nonlinearities in signal transformations will be interpreted as additional noise and uncertainties. Nevertheless, some nonlinearities can be eliminated. For example, sometimes the shift-invariant blur process is modeled by the Equation [27]:

$$w(x) \approx c(u * v)(x),$$

where $c(x)$ is some nonlinear function. If the function $c(x)$ has an inverse $c^{-1}(x)$, then the equation $c^{-1}w(x) \approx (u * v)(x)$ describes the LS system without nonlinearity.

Note that within the framework of TT methods, it is quite easy to consider any kind of LS system actions and reactions. These can be electrical signals or physical fields acting on, measured, transmitted, or generated by the processing system. The only thing to do is to use the appropriate types of actions and reactions of the test trials. Moreover, when TSs are determined experimentally, there is no need to analyze the LS system and parasitic parameters of its elements, since this information is provided in the TSs. This allows recovering signals of high-speed and precise processing systems of almost any complexity and structure.

7. Conclusions

Mathematical methods for non-blind reconstruction of multidimensional signals and images distorted and noisy during their processing by LS systems are proposed and analyzed. Instead of transfer functions, which are often difficult to determine because they belong to the class of generalized functions, the proposed TT methods use test trial signals of processing systems. The signals belong to the class of ordinary functions, which allows the efficient use of many existing methods, such as regularization techniques, to solve ill-posed and ill-conditioned reconstruction problems.

The test trials of the processing systems are in fact their extended calibration or their dynamic calibration in the one-dimensional case. This extended calibration determines the accuracy of the TT method, the stability of its algorithm, and the possibility of improving the effective parameters of the processing systems.

The proposed operator approach based on the multidimensional convolution equation significantly increases the speed of numerical computations. The considered method allows improving the quality of signal and image processing without complex and expensive modernization of the equipment.

Recommendations

The proposed TT approach allows to expand the scope of application of mathematical reconstruction methods, so it has a wide area of practical application. They enable to improve the quality of signal and image processing without complex and expensive modernization of equipment.

Within the framework of TT methods, it is possible to consider any kind of LS system actions and reactions by simply using the appropriate types of test actions and reactions.

When TSs are determined experimentally, there is no need to analyze the LS system and parasitic parameters of its elements, since this information is provided in the TSs. This allows recovering signals of high-speed and precise processing systems of almost any complexity and structure.

Acknowledgements

The author is grateful to the management of the Experimental Physics Department of the Institute for Nuclear Research of the Russian Academy of Sciences for support of this work.

Funding Support

This work was supported by ongoing institutional funding within the framework of the state fundamental scientific research on the topics: 1.1.2.2. Inverse and ill-posed problems, methods of data assimilation; 1.3.2.11. Fundamental problems of physical electronics; 1.3.3.1. Physics of elementary particles and fundamental interactions; 1.3.3.6. Development of methods of detection of elementary particles, atomic nuclei, and ionizing radiation, methods of X-ray and neutron optics; 1.3.6.2. Development of methods of generation, amplification, conversion, and reception of electromagnetic waves. No additional grants to carry out or direct this particular research were obtained.

Ethical Statement

This study does not contain any studies with human or animal subjects performed by any of the authors.

Conflicts of Interest

The author declares that he has no conflicts of interest to this work.

Data Availability Statement

The data that support the findings of this study are openly available in GitHub at https://github.com/novikov-borodin/data-rec.

Author Contribution Statement

Andrey V. Novikov-Borodin: Conceptualization, Methodology, Software, Validation, Formal analysis, Investigation, Resources, Data curation, Writing – original draft, Writing – review & editing, Visualization, Project administration, Funding acquisition.

References

[1] Kazufumi, I., & Bangti, J. (2014). *Inverse problems: Tikhonov theory and algorithms*. Singapore: World Scientific.

[2] Chassain, C., Kusiak, A., Krause, K., & Battaglia, J. L. (2024). Optimal experiment design for inverse problems via selective normalization and zero-shift times. *Journal of Inverse and Ill-posed Problems*, *32*(6), 1129–1140. https://doi.org/10.1515/jiip-2023-0063

[3] Chung, E., Ito, K., & Yamamoto, M. (2021). Least squares formulation for ill-posed inverse problems and applications. *Applicable Analysis*, *101*(15), 5247–5261. https://doi.org/10.1080/00036811.2021.1884228

[4] Liang, Y., Gao, X. W., Xu, B. B., Cui, M., & Zheng, B. J. (2020). A reduced-order modelling for real-time identification of damages in multi-layered composite materials. *Inverse Problems in Science and Engineering*, *29*(1), 73–94. https://doi.org/10.1080/17415977.2020.1775826

[5] Sobolev, V. I. (2001). *Convolution of functions, encyclopedia of Mathematics*. Finland: EMS Press.

[6] Chaganova, O. B., Grigoryev, A. S., Nikolaev, D. P., & Nikolaev, I. P. (2024). Applied aspects of modern non-blind image deconvolution methods. *Computer Optics*, *48*(4), 562–572. https://doi.org/10.18287/2412-6179-CO-1409

[7] Chen, M., Quan, Y., Pang, T., & Ji, H. (2022). Nonblind image deconvolution via leveraging model uncertainty in an untrained deep neural network. *International Journal of Computer Vision*, *130*, 1770–1789. https://doi.org/10.1007/s11263-022-01621-9

[8] Quan, Y., Chen, Z., Zheng, H., & Ji, H. (2022). Learning deep non-blind image deconvolution without ground truths. In S. Avidan, G. Brostow, M. Cissé, G. M. Farinella, & T. Hassner (Eds.), *Computer vision: ECCV 2022. ECCV 2022.*

Lecture notes in computer science, vol *13666*. Switzerland: Springer. https://doi.org/10.1007/978-3-031-20068-7_37

[9] Lim, S., Park, H., Lee, S. E., Chang, S., Sim, B., & Ye, J. C. (2020). CycleGAN with a blur kernel for deconvolution microscopy: Optimal transport geometry. *IEEE Transactions on Computational, Imaging*, *6*, 1127–1138. https://doi.org/10.48550/arXiv.1908.09414

[10] Schuler, C. J., Burger, H. C., Harmeling, S., & Schölkopf, B. (2013). A machine learning approach for non-blind image deconvolution. In *Proceedings of the IEEE Conference on Computer Vision and Pattern Recognition*. https://doi.org/10.1109/CVPR.2013.142

[11] Liu, X., Wu, Z., & Wang, X. (2023). The validity analysis of the non-local mean filter and a derived novel denoising method. *Virtual Reality & Intelligent Hardware*, *5*(4), 338–350. https://doi.org/10.1016/j.vrih.2022.08.017

[12] Wang, H., Zhang, J., Dong, X., Wang, T., Ma, X., & Wang, J. (2024). Ambulatory ECG noise reduction algorithm for conditional diffusion model based on multi-kernel convolutional transformer. *The Review of Scientific Instruments*, *95*(9), 95–107. https://doi.org/10.1063/5.0222123

[13] Guo, X., Liu, F., & Tian, X. (2021). Gaussian noise level estimation for color image denoising. *Journal of the Optical Society of America A*, *38*(8), 1150–1159. https://doi.org/10.1364/JOSAA.426092

[14] Wang, H., Sreejith, S., Lin, Y., Ramachandra, N., Slosar, A., & Yoo, S. (2022). Neural network based point spread function deconvolution for astronomical applications. *arXiv Preprint: 2210.01666*.

[15] Li, T., Tian, M., Gao, C., & Sang, N. (2025). Self-distilled dual-network with pixel screening loss for blind image deblurring. In A. Antonacopoulos, S. Chaudhuri, R. Chellappa, C. L. Liu, S. Bhattacharya, & U. Pal (Eds.), *Pattern recognition. ICPR 2024. Lecture notes in computer science* (vol. *15332*, pp. 167–181). Switzerland: Springer. https://doi.org/10.1007/978-3-031-78125-4_12

[16] Zhang, M., Fang, Y., Ni, G., & Zeng, T. (2022). Pixel screening based intermediate correction for blind deblurring. In *Proceedings of the IEEE/CVF Conference Computer Vision Pattern Recognition*, 5892–5900. https://doi.org/10.1109/CVPR52688.2022.00580

[17] Junjie, T. A. O., Yinghui, W. A. N. G., Haomiao, M. A., Tao, Y. A. N., Lingyu, A. I., & Wei, L. I. (2023). Image defocus deblurring method based on gradient difference of boundary neighborhood. *Virtual Reality & Intelligent Hardware*, *5*(6), 538–549. https://doi.org/10.1016/j.vrih.2023.06.008

[18] Jo, H., Son, H., Hwang, H. J., & Kim, E. (2020). Deep neural network approach to forward-inverse problems. *Networks and Heterogeneous Media*, *15*(2), 247–259. https://doi.org/10.3934/nhm.2020011

[19] Isaev, I., Obornev, I., Obornev, E., Rodionov, E., Shimelevich, M., & Dolenko, S. (2022). Integration of geophysical methods for solving inverse problems of exploration geophysics using artificial neural networks. In A. Kosterov, N. Bobrov, E. Gordeev, E. Kulakov, E. Lyskova, & I. Mironova (Eds.), *Problems of Geocosmos–2020. Springer proceedings in earth and environmental sciences*. Switzerland: Springer. https://doi.org/10.1007/978-3-030-91467-7_7

[20] Jung, Y., Kong, J., Sheng, B., & Kim, J. (2024). A transfer function design for medical volume data using a knowledge database based on deep image and primitive intensity profile features retrieval. *Journal of Computer Science and Technology*, *39*(9), 320–335. https://doi.org/10.1007/s11390-024-3419-7

[21] Li, J., Zhang, P., Wang, T., Zhu, L., Liu, R., Yang, X., . . . , & Sheng, B. (2024). DSMT-Net: Dual self-supervised multi-operator transformation for multi-source endoscopic ultrasound diagnosis. *IEEE Transactions on Medical Imaging*, *43*(1), 64–75.

[22] Elsayed, M. A., El-Shafai, W., Rashwan, A. M., Dessouky, M. I., El-Fishawy, A. S., & Abd El-Samie, E. F. (2023). Efficient iterative implementation of regularized solutions for image and signal reconstruction problems. *Journal of Optics*, *53*, 1–11. https://doi.org/10.1007/s12596-023-01179

[23] Xiao, Z., Fang, H., Tomasin, S., Mateos, G., & Wang, X. (2023). Joint sampling and reconstruction of time-varying signals over directed graphs. *IEEE Transactions on Signal Processing*, *71*, 2204–2219. https://doi.org/10.1109/TSP.2023.3284364

[24] Novikov-Borodin, A. V. (2023). Test methods for signal reconstruction of linear stationary systems. *Journal of Communications Technology and Electronics*, *68*(7), 732–747. https://doi.org/10.1134/S1064226923070082

[25] Novikov-Borodin, A. V. (2022). Reconstruction and simulation of experimental data using test measurements. *Instruments and Experimental Techniques*, *65*(2), 238–245. https://doi.org/10.1134/S0020441222020166

[26] Malay, I. (2023). Digital signal processing in modern radio engineering measurements. In *Plenary Talk at XXV International Conference Digital Signal Processing and Its Applications*.

[27] Ren, W., Zhang, J., Ma, L., Pan, J., Cao, X., Zuo, W., . . . , & Yang, M. H. (2018). Deep non-blind deconvolution via generalized low-rank approximation. In *Advances in Neural Information Processing Systems: 32nd Conference on Neural Information Processing Systems*, 295–305. https://doi.org/10.5555/3326943.3326971

How to Cite: Novikov-Borodin, A. V. (2025). Using Test Trials of Processing Systems for Non-Blind Recovery of Signals and Images. *Journal of Data Science and Intelligent Systems*. https://doi.org/10.47852/bonviewJDSIS52024990